

Flexural behavior of titanium bar reinforced granite with various reinforcement ratio

Woo-Young Lim*

Department of Architectural Engineering, Wonkwang University, 460 Iksandae-ro, Iksan 54538, South Korea

(Received November 4, 2019, Revised January 6, 2020, Accepted January 21, 2020)

Abstract. Granite is commonly used in the construction of the ancient stone pagodas of Korea. The material has excellent weathering resistance and durability, as well as high compressive strength. Most of the stone-made state-designated architectural heritage of Korea is made of granite. Therefore, the understanding of the structural feasibility of stone-made architectural heritage is crucial. Even though, until now, experimental studies for the reinforced stone have been rarely performed. This study intends to suggest a new methodology for the reinforcement of granite using a threaded titanium bar. Through the experimental study, the flexural behavior of the reinforced granite depending on the reinforcement ratio is investigated. Based on the test results, a moment–displacement relationship for the design of reinforced granite is suggested.

Keywords: restoration; ancient stone pagoda; granite; titanium bar; flexural behavior; reinforcement ratio;

1. Introduction

Granite is one of the stones widely used in the construction of the ancient stone pagoda of Korea. The material has excellent weathering resistance, abundant reserves, durability, and high compressive strength. According to the investigation, approximately 50% of the stone-made state-designated architectural heritage of Korea is made of granite (National Research Institute of Cultural Heritage 2014).

Among the stone pagodas made of granite, the most famous stone pagoda is the Mireuksaji stone pagoda, which is located at the Mireuksa temple site in Iksan, Jeonbuk province [Fig. 1(a)]. This pagoda is the oldest and largest stone pagoda (14.5 m height and 12.5 m width) in Korea. Historical documents said that the pagoda was built at the end of the Korean kingdom of Baekje in 639. As shown in Figs. 1(b) and (c), the pagoda was originally a 9-floor structure, but the whole of the west side, most of the southern side, and half of the northern side collapsed; currently, only six floors remain. The collapsed part has been covered with concrete, as depicted in Fig. 1(c).

According to the structural safety diagnosis for the stone pagoda performed in 1998, the durability of the concrete was remarkably reduced, so the stone pagoda was found to be structurally unstable (Korea Institute of Construction Safety Technology 1998). Based on the assessment of structural performance, eventually, the Cultural Properties Committee decided to re-assemblage the stone pagoda after the dismantlement of all the elements in 1999.

Restoration of the stone pagoda was carried out according to the following procedure. First, the concrete

was removed, and the stone pagoda dismantled into all of its components [Figs. 1(d) and (e)]. The damaged members were then repaired and reinforced with new granite. To reinforce the damaged granite, several preconditions are required. Granite used for restoration should have the same material properties as the existing granite. According to previous research, granite mined in the Hwangdeong area located near Mireuksan at Iksan in Jeonbuk Province was found to be mostly identical to the granite used in the stone pagoda (Yang *et al.* 2006, Kim *et al.* 2011) [Fig. 1(a)]. Additionally, the repaired granite should have resistance for the self-weight and gravity load to prevent the collapse of the stone pagoda due to excessive load. Finally, sufficient bond strength at the interface between old and new granite is needed.

To reinforce the granite, this study uses the threaded titanium bar as the reinforcement. Metal rods have been used in the reinforcement of stone-made cultural heritage for a long time. Initially, carbon steel was mainly used for stone reinforcement, but recently it is being replaced by new metals such as titanium to prevent corrosion of the metal reinforcement. It is known that titanium has a lower modulus of elasticity than stainless or carbon steel, but has small specific gravity, small thermal conductivity, small thermal expansion coefficient, and excellent corrosion resistance. Recently, T-shaped titanium clamps have been used to reinforce marble in the Greek Parthenon restoration project (Zambas *et al.* 1986, Zambas 1992). Recently, the research on the seismic behavior, collapse mechanism, and nonlinear analysis of historic structures have been conducted (Kocatürk *et al.* 2016, Demir *et al.* 2016, Nohutcu *et al.* 2017, Hamdy *et al.* 2018) but experimental studies for the reinforced granite for restoration of the ancient stone pagoda have been rarely performed.

This study intends to suggest a new methodology for the reinforcement of granite using a threaded titanium bar. Flexural tests for reinforced granite are performed to verify

*Corresponding author, Ph.D., Assistant Professor
E-mail: wylim97@wku.ac.kr



(a) Location of the Mireuksa Temple Site



(b) The eastern and western side of the stone pagoda in 1910 (Photo courtesy of the National Archives of Korea) (c) The southeastern side of the stone pagoda (Photo courtesy of Jeonbuk Provincial Government)



(d) The disassembly of the first tier of the stone pagoda in 2008 (Photo courtesy of the Iksan National Museum of Korea) (e) The reassembly of the sixth tier in 2017 (Photo courtesy of the Iksan National Museum of Korea)

Fig. 1 Restoration of the Mireuksaji stone pagoda

the structural feasibility of the proposed method. Through the experimental study, the flexural behavior of the reinforced granite with various reinforcement ratio is investigated.

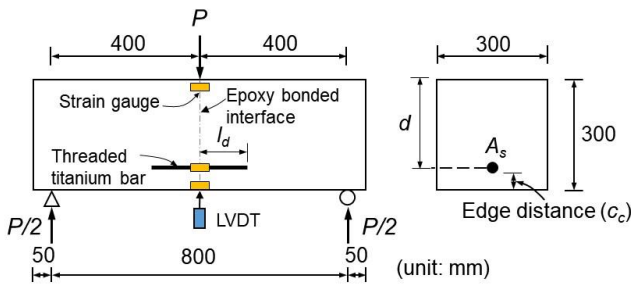
2. Test program

2.1 Details of the test specimen

Figure 2 shows the configuration of the specimen with dimensions of 300 mm × 300 mm × 900 mm (width × height × length). To manufacture the test specimens, granite supplied at the Hwangdeung quarry was used. For the reinforcement, titanium bars [Grade 2 ($f_y = 313.8$ MPa and $f_u = 431.5$ MPa)] with a length of 400 mm (embedment

length = 200 mm) were used, where f_y and f_u are the design yield and tensile strength of the reinforcement, respectively. For perfect bonding between the reinforcing bar and epoxy resin, a thread with a depth of 1 mm was placed on the reinforcing bar. Here, the embedment length of the reinforcing bar was obtained according to Section 25.4 of the ACI 318-14 (2014). The bar was inserted into the drilled hole after the injection of the epoxy resin.

The test parameters are the bar diameter (d_b) and edge distance (e). In this test, threaded titanium bars with diameters of 8 to 25 mm were used. The edge distance is 20 to 90 mm, depending on the bar diameter by Section 20.6.1 of ACI 318-14 (2014). According to ACI 318-14 (2014), when a bar diameter is greater than 29 mm, the edge distance of 60 mm should be allowed. If the bar diameter is less than 25 and 16 mm, the distance must meet a minimum



(a) Configuration of the test specimen



(b) Threaded titanium bar

Fig. 2 Details of the test specimens and measurement



Fig. 3 Test setup

of 50 and 40 mm, respectively. Thus, the reinforcement ratio is ranged from 0.061 to 0.828%.

In total, 39 specimens were tested. Table 1 presents detailed information about the test specimen. The CEP specimen is a control specimen that is bonded only with epoxy resin. Except for the CEP, all the specimens are reinforced granite.

2.2 Test setup

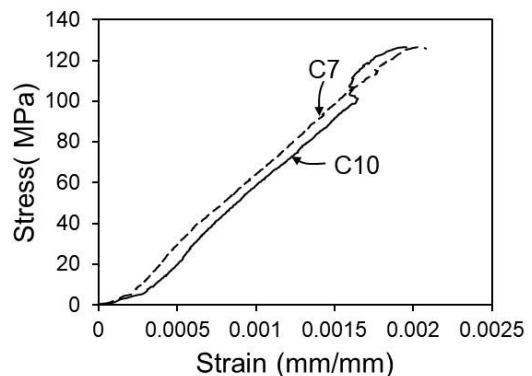
Three-point bending tests for simply supported reinforced granite were performed using an actuator with a capacity of 1,000 kN under displacement control, in accordance with ASTM C78/C78M-18 (2018). Figure 3 shows the test setup. During the test, the load was applied at a rate of 0.3 mm/min. The displacement was measured using a Linear Variable Differential Transducer (LVDT) mounted at the bottom of the specimen. The strain of granite was measured using strain gauges placed at the distance of 30 mm from the extreme fiber of the upper and lower part of the test specimen. The strain of the titanium bar was obtained by the strain gauge placed at the mid-length of the bar (Fig. 2).

2.3 Material properties

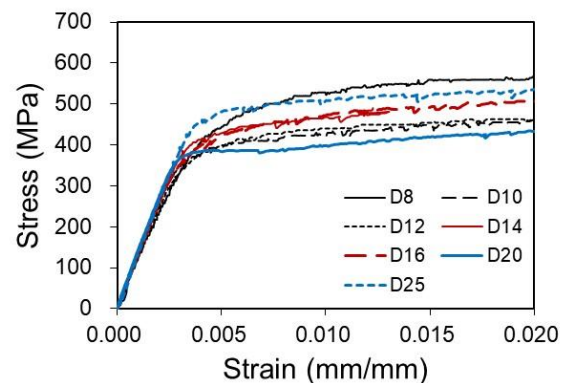
2.3.1 Compression tests of granite

Compression tests were conducted for the ten cubic granite specimens with dimensions of 50 mm × 50 mm × 50 mm using a universal testing machine with a capacity of 2,000 kN in accordance with ASTM C1194-18 (2018) and KS F 2519 (2015). From the test results, the peak compressive strength, strain corresponding to the peak compressive strength, and elastic modulus of granite were investigated. To obtain the stress–strain relationship, the axial strains were measured by two strain gauges attached to the front and backside surface of the specimens.

Figure 4(a) shows the stress–strain relationship of granite under uniaxial compression. It is noted that a total of 10 cubic granite were tested, but significant stress–strain curves were obtained in two specimens (C7 and C10 specimen). In this study, the material properties of granite were defined using the results obtained from these two specimens. The specimens showed linear-elastic behavior, and brittle failure occurred when the strength reached the peak value. The compressive strength of granite was found to be 72.2 to 146.4 MPa, with an average strength of 131.7 MPa. The compressive strains of C7 and C10 specimens at the ultimate state were found to be 0.0021 and 0.002, respectively. The elastic modulus (E_g) of granite was obtained by dividing the 40% of the peak stress (f_{cg}) with the strain corresponding to the $0.4f_{cg}$ in accordance with EN 1992-1-1 (2004). The average elastic modulus of granite was found to be 58.6 GPa.



(a) Compressive stress-strain curve



(c) Tensile stress-strain curve

Fig. 4 Material tests

Table 1 Summary of test results

Speci -mens	d_b (mm)	e (mm)	ρ (%)	P_{el} (kN)	$\Delta@P_{el}$ (mm)	P_{min} (kN)	$\Delta@P_{min}$ (mm)	P_{ult} (kN)	$\Delta@P_{ult}$ (mm)	P_f (kN)	$\Delta@P_f$ (mm)	μ	P_{el} / P_{CEP}	P_{min} / P_{el}	P_{ult} / P_{el}	FM
CEP	-	-	-	267.1	N.A.	-	-	-	-	-	-	-	-	-	-	F
SP8-20	8	20	0.061	189.1	0.48	7.1	2.26	27.7	2.64	18.4	4.52	2.00	0.71	0.04	0.15	F
SP8-30	8	30	0.063	220.5	0.48	4.3	2.50	25.2	3.71	14.7	5.55	2.22	0.83	0.02	0.11	F
SP8-40	8	40	0.065	229.5	0.39	3.7	2.44	26.5	2.85	16.0	3.41	1.40	0.86	0.02	0.12	F
SP8-50	8	50	0.068	216.6	0.39	5.5	2.62	23.4	3.25	14.3	5.19	1.98	0.81	0.03	0.11	F
SP8-60	8	60	0.071	197.8	0.49	3.7	2.67	12.1	3.75	2.4	7.94	2.97	0.74	0.02	0.06	F
SP8-70	8	70	0.074	223.8	0.49	2.5	2.71	19.9	3.66	6.8	5.87	2.17	0.84	0.01	0.09	F
SP10-20	10	20	0.095	241.8	0.44	22.0	2.26	40.6	3.34	33.4	4.53	2.00	0.91	0.09	0.17	F
SP10-30	10	30	0.099	210.4	0.48	12.2	2.17	34.0	2.92	9.3	6.25	2.88	0.79	0.06	0.16	F
SP10-40	10	40	0.103	222.2	0.35	3.9	2.27	28.0	3.00	23.8	3.83	1.69	0.83	0.02	0.13	F
SP10-50	10	50	0.107	229.3	0.39	22.1	2.28	40.7	2.91	33.9	5.08	2.23	0.86	0.10	0.18	F
SP10-60	10	60	0.111	226.9	0.38	22.7	2.49	41.9	3.87	30.5	6.91	2.78	0.85	0.10	0.18	F
SP10-70	10	70	0.116	280.3	0.61	13.5	2.96	44.0	4.07	23.3	4.62	1.56	1.05	0.05	0.16	F
SP12-40	12	40	0.148	211.0	0.38	60.2	1.33	72.4	2.88	68.3	3.23	2.43	0.79	0.29	0.34	F+S
SP12-50	12	50	0.155	227.7	0.62	54.1	1.71	74.5	4.08	67.4	5.15	3.01	0.85	0.24	0.33	F
SP12-60	12	60	0.161	211.5	0.51	58.7	1.43	71.3	2.13	59.6	5.37	3.76	0.79	0.28	0.34	F
SP12-70	12	70	0.168	250.8	0.51	48.1	2.10	65.7	2.58	60.8	4.96	2.36	0.94	0.19	0.26	F
SP12-80	12	80	0.176	217.3	0.52	52.3	1.74	73.7	2.68	70.8	5.41	3.11	0.81	0.24	0.34	F
SP14-40	14	40	0.203	211.0	0.51	75.6	1.28	82.5	2.63	63.7	5.79	4.52	0.79	0.36	0.39	F
SP14-50	14	50	0.211	210.1	0.47	68.3	1.38	83.4	2.85	65.4	8.77	6.36	0.79	0.33	0.40	F
SP14-60	14	60	0.220	211.9	0.66	88.1	1.35	102.3	3.36	92.4	6.04	4.47	0.79	0.42	0.48	F
SP14-70	14	70	0.230	259.7	0.45	65.8	1.64	89.4	5.25	88.1	4.42	2.70	0.97	0.25	0.34	F
SP14-80	14	80	0.241	231.0	0.57	74.3	1.48	91.4	3.58	84.7	5.17	3.49	0.86	0.32	0.40	F
SP16-40	16	40	0.266	219.5	0.39	123.7	1.03	137.9	2.08	127.3	2.40	2.33	0.82	0.56	0.63	F+S
SP16-50	16	50	0.277	260.9	0.43	109.0	1.15	129.2	2.44	125.4	2.57	2.23	0.98	0.42	0.50	F+S
SP16-60	16	60	0.289	254.2	0.47	106.2	1.31	125.4	1.93	114.7	9.33	7.12	0.95	0.42	0.49	F
SP16-70	16	70	0.302	205.6	0.47	97.2	1.06	128.1	2.56	119.7	8.05	7.59	0.77	0.47	0.62	F
SP16-80	16	80	0.316	235.3	0.34	101.0	1.21	114.1	3.87	101.4	6.60	5.45	0.88	0.43	0.48	F
SP16-90	16	90	0.332	223.0	0.50	95.3	1.18	122.2	4.71	114.8	7.80	6.61	0.83	0.43	0.55	F
SP18-40	18	40	0.338	183.7	0.46	113.9	0.87	150.5	2.55	145.0	2.62	3.01	0.69	0.62	0.82	F+S
SP18-50	18	50	0.352	227.6	0.60	111.5	1.21	156.9	5.68	122.9	9.64	7.97	0.85	0.49	0.69	F
SP18-60	18	60	0.367	236.1	0.47	109.6	1.38	143.1	5.58	76.4	7.05	5.11	0.88	0.46	0.61	F
SP18-70	18	70	0.384	257.6	0.51	109.5	1.34	158.2	6.34	108.7	9.72	7.25	0.96	0.43	0.61	F
SP18-80	18	80	0.402	220.9	0.61	97.7	1.31	132.4	7.61	96.6	9.04	6.90	0.83	0.44	0.60	F
SP18-90	18	90	0.422	194.0	0.46	97.1	1.01	122.5	5.50	95.3	9.21	9.12	0.73	0.50	0.63	F
SP20-80	20	80	0.499	234.9	0.49	125.0	1.16	171.2	5.35	165.0	7.68	6.62	0.88	0.53	0.73	F
SP20-90	20	90	0.524	222.5	0.51	116.5	1.16	163.2	9.02	92.9	12.72	10.97	0.83	0.52	0.73	F
SP25-80	25	80	0.789	260.2	0.53	164.1	1.06	198.6	2.51	189.0	2.58	2.43	0.97	0.63	0.76	F+S
SP25-90	25	90	0.828	253.1	0.48	138.7	1.14	185.5	2.18	177.7	2.24	1.96	0.95	0.55	0.73	F
												Avg.	0.85 [†]	0.30 [†] (0.40 [*])	0.41 [†] (0.51 [*])	
												S.D.	0.08 [†]	0.20 [†] (0.11 [*])	0.23 [†] (0.15 [*])	

Notes: d_b is the bar diameter, e is the edge distance, ρ is the reinforcement ratio ($= A_s/bd$), A_s is the area of the reinforcement, b is the width of the specimen, d is the effective depth of the specimen ($= h-e-d_b/2$), and h is the overall height. μ is the ductility ($= \Delta@P_{min}/\Delta@P_f$). FM means the Failure Mode; F and S represent the flexural and shear failure, respectively.

[†] For all the test results.

^{*} For the reinforcement ratio ranged from 0.148% (SP12-40) to 0.524% (SP20-90).

2.3.2 Tension tests of titanium bars

Tension tests for 15 round titanium bars (Grade 2) were carried out using a 2,000 kN UTM in accordance with ASTM E8/E8M (2016). For the tests, two specimens for each (D8 to D22) ($d_b = 8$ to 22 mm) bar, and one specimen for the D25 bar were tested.

Figure 4(b) shows the stress–strain curves of the titanium round bars. The elastic modulus is defined as the slope of the straight line connecting the yield strength and the yield strain obtained by 0.2% offset in the stress–strain curve. Test results are summarized in Table 2.

2.3.3 Adhesives and fillers

Epoxy resin has been widely used as adhesive in historic architectural structures (Selwitz 1992). For the adhesion of old and new granite, thermosetting epoxy resin (L30) produced by P Company of Korea was used. The characteristics of the adhesive are that it has a small shrinkage force, does not have an additive product according to the reaction, and is easy to work. Still, it does have the disadvantage that yellowing occurs with time. A filler was added to the epoxy resin. In this study, zirconium silicate, wollastonite, and talc were used as the filler. Zirconium silicate was used to prevent chemical weathering

Table 2 Material properties of the titanium bar

Specimens	f_y (MPa)	ε_y (mm/m m)	f_u (MPa)	ε_u (mm/m m)	E_s (GPa)
D8	440.5	0.0049	568.6	0.0237	89.9
D10	383.1	0.0042	460.5	0.0252	91.2
D12	390.5	0.0049	485.0	0.0720	79.7
D14	405.9	0.0042	443.9	0.0735	96.6
D16	412.6	0.0045	517.7	0.0246	91.7
D18	356.8	0.0033	456.4	0.0300	108.1
D20	374.2	0.0036	457.7	0.0314	103.9
D25	451.8	0.0041	540.4	0.0237	110.2

Notes: The symbols of the f_y and f_u are yield and tensile strengths of the titanium bar, ε_y and ε_u are strains corresponding to f_y and f_u , respectively.

Table 3 Physical properties of the epoxy resin

Tests	Resin L-30R	Hardener L-30H
Appearance	Clear	Clear
Viscosity (cps) 25 °C	300 ~ 400	230 ~ 300
Specific gravity	1.20	0.97
Mixing Ratio	100	500
Pot Life (100g) 25 °C	30 ~ 40 min.	
Curing schedule 25 °C	Physical cure 24hrs Chemical cure 7days	
Shear adhesive strength	60% filled type 17.17 N/mm ² Nonfilled type 10.49 N/mm ²	

and metamorphism. Moreover, wollastonite was used for improving the impact resistance and tensile strength, and talc for flow prevention and improvement of adhesion. Table 3 summarizes the physical properties of the epoxy resin.

3. Test results

3.1 Failure mode

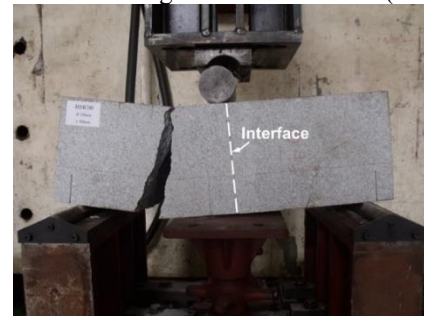
In most of the specimens, initial flexural cracking occurred at the interface, and the crack propagated to the top of the specimen very rapidly with the increase of load. Subsequently, tensile resistance by the titanium reinforcing bar started to take place after the beginning of initial cracking [Fig. 5(a)]. As the crack width increased, the strain of the reinforcing bar increased very rapidly; and finally, the bars reached the ultimate state. However, in some test specimens reinforced with D8, D10, D12, D14, D16, and D18 titanium bars, bar fracture occurred before the yield state. Several test specimens (SP12-40, SP16-40, SP16-50, SP18-40, and SP25-80 specimens) showed diagonal tension failure. Figure 5(b) shows the diagonal tension failure of the SP16-50 specimen. The diagonal tension cracks occurred at



(a) Flexural crack and bar fracture (SP20-90)



(b) Flexural and diagonal tension failure (SP16-50)



(c) Failure mode of SP25-90 specimen

Fig. 5 Failure mode of the test specimens at the end of the tests

the distance of development length (= 200 mm) of the bar. In the case of SP25-90 specimen, a flexural crack occurred at the distance of the development length of the bar from the interface [Fig. 5(c)]. However, bond splitting failure at the edge distance did not occur in all the test specimens.

The most notable feature of the failure mode of reinforced granite is that critical crack occurs immediately as soon as the initial crack initiated. Additionally, diagonal tension failure can occur in specimens with relatively low reinforcement ratios.

3.2 Load-displacement relationship

Figure 6 shows the load-displacement curves of the reinforced granite. Test results demonstrated that the load-deflection relationships of reinforced granite were highly dependent on the reinforcement ratio and edge distance. Furthermore, the flexural behavior of the reinforced granite seems to follow a similar pattern. Thereby, the load-displacement relationship of the reinforced granite can be idealized, as shown in Fig. 7; the elastic state (Stage I), reinforcing bar yielding (Stage II), strain hardening (Stage III), and strain softening of reinforcing bar and fracture (Stage IV).

All the specimens showed linear-elastic behavior before reaching the elastic limit. In most of the reinforced

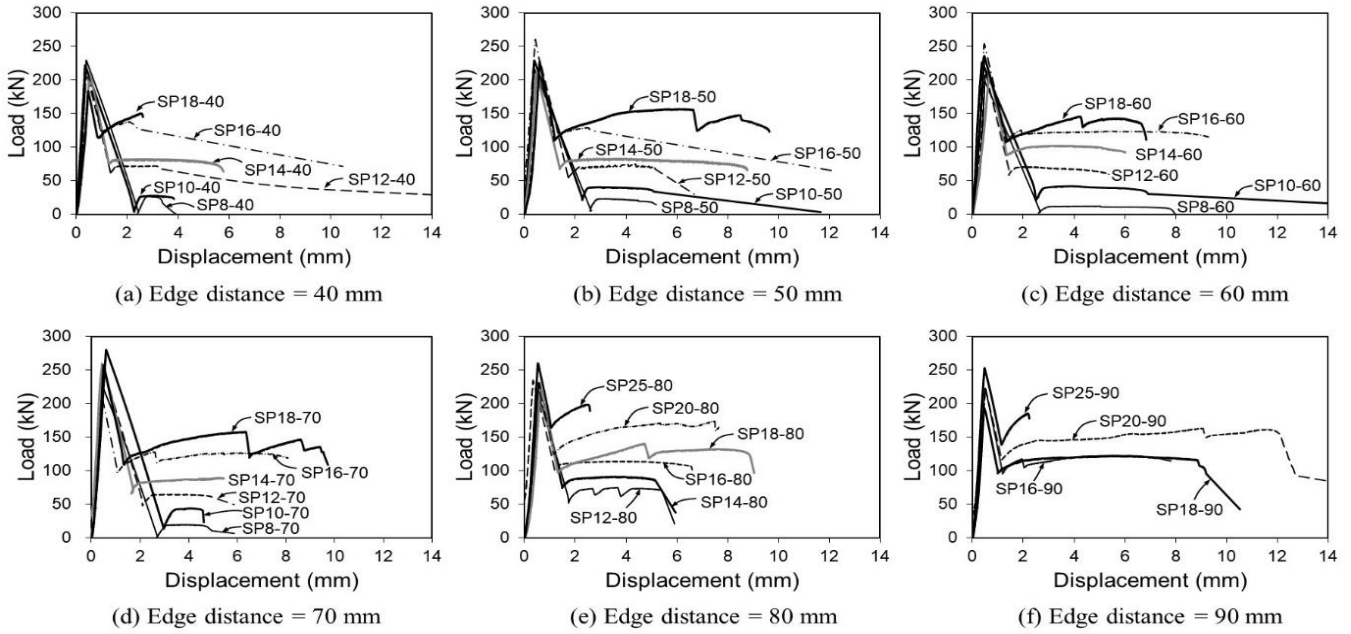
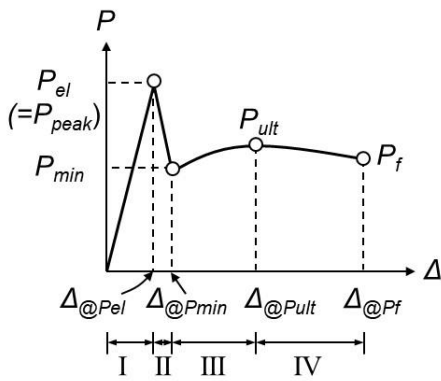
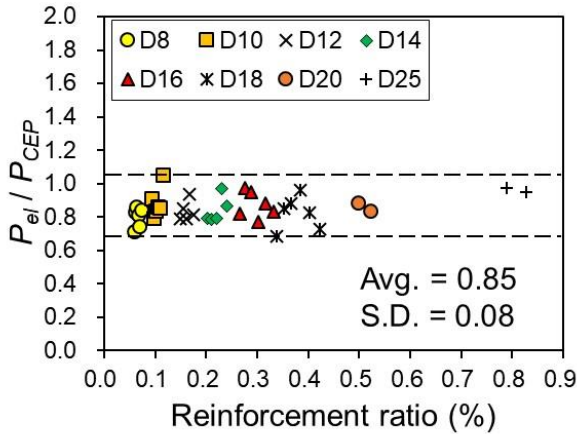


Fig. 6 Load-displacement relationship

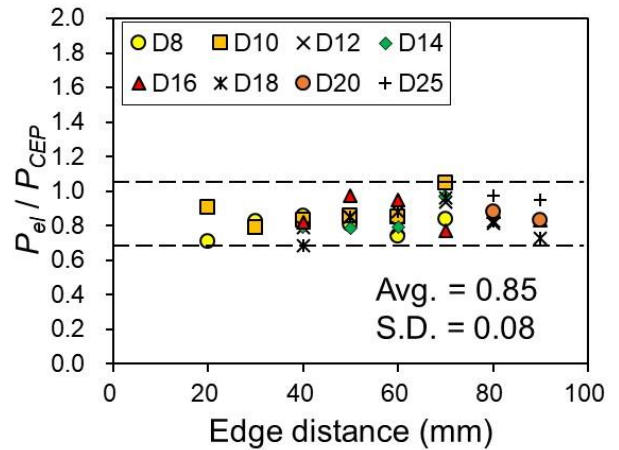


- Stage I: Elastic state
- Stage II: Reinforcing bar yielding after flexural cracking
- Stage III: Strain hardening of reinforcing bar
- Stage IV: Strain softening of reinforcing bar and a failure

Fig. 7 Idealized load-displacement relationship



(a) For reinforcement ratio



(b) For edge distance

Fig. 8 Ratio of the load in the elastic state between the reinforced and control specimens

specimens, a sudden drop of load occurred as soon as the load reached the elastic limit, but it subsequently increased again due to the strain hardening of the reinforcing bar, reached the ultimate load, and gradually decreased with the elongation of the reinforcing bars. Finally, the tests were terminated by bar fracture. In this study, the symbols of P_{el} , P_{min} , P_{ult} , and P_f are defined as the load at the elastic limit, minimum load resistance, ultimate load resistance, and load at failure, respectively. The displacements corresponding to P_{el} , P_{min} , P_{ult} , and P_f are represented by $\Delta_{@P_{el}}$, $\Delta_{@P_{min}}$, $\Delta_{@P_{ult}}$, and $\Delta_{@P_f}$, respectively.

The test results showed that when the edge distance ranged 40 to 80 mm, and the reinforcement ratio was less than approximately 0.3% (D16) after the initial crack occurred, there was almost no increase in load. On the other hand, when the reinforcement ratio exceeded 0.3%, the increase in the load was apparent, due to the tensile

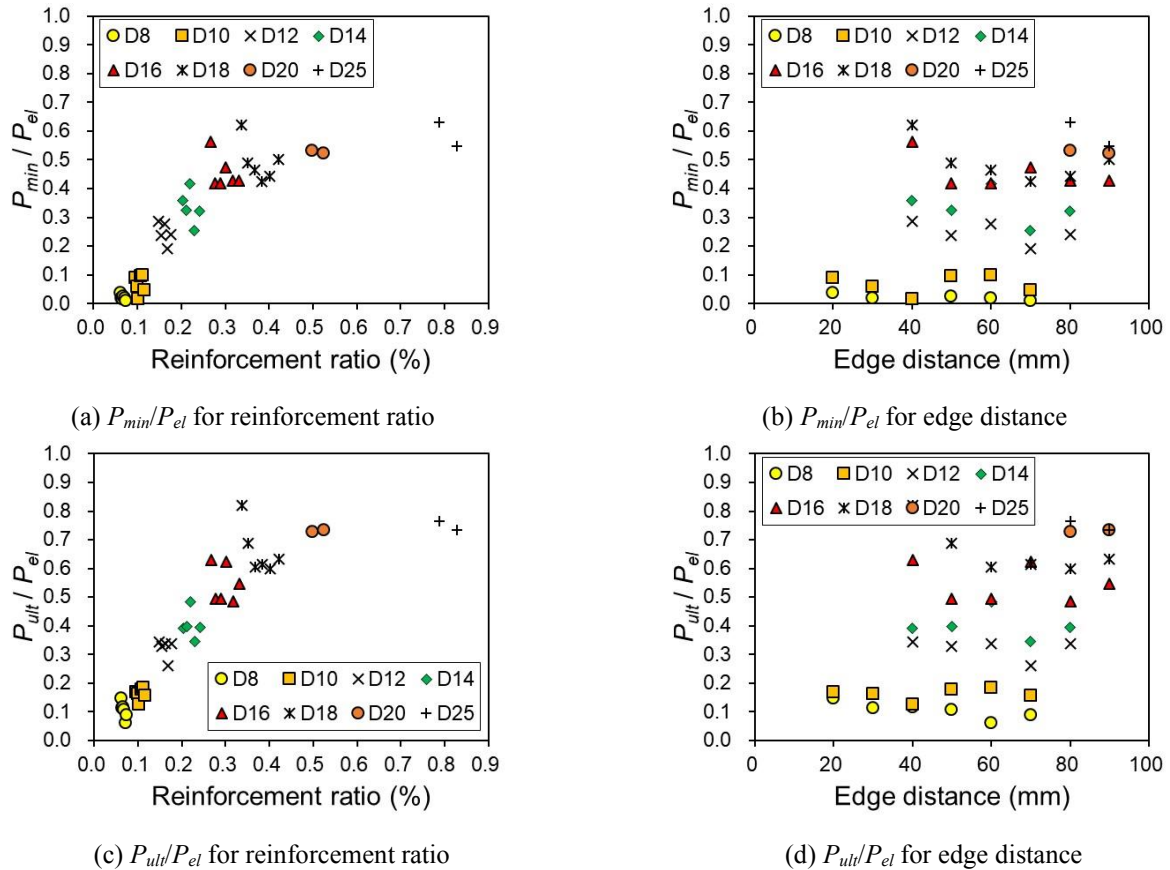


Fig. 9 Comparisons of the minimum and ultimate load resistance to the load in the elastic state

resistance of the titanium bar. When the edge distance was 90 mm, and the reinforcement ratio was less than 0.422% (SP18-90), the load did not increase further; and when the reinforcement ratio was greater than 0.499% (SP20-90), the load increased again.

The elastic loads of all the specimens were very similar to each other. This means that the measured elastic loads were not significantly affected by the reinforcement ratio and edge distance. Figure 8 compares the elastic load between reinforced and control specimen. The ratio ranged from 0.69 to 1.05, and the average value of the ratio was 0.85, with a standard deviation of 0.08. The elastic load of the reinforced granite was slightly smaller than that of the CEP specimen, probably because of the presence of fine cracks at the junction between the epoxy and cracked surface of the granite.

Figure 9 compares the minimum and ultimate load resistance to the load in the elastic state. The minimum load resistance (P_{min}) was substantially dependent on the reinforcement ratio and increased as the reinforcement ratio increased [Fig. 9(a)]. However, when the reinforcement ratio was more than 0.3%, the value of P_{min} tended to decrease gradually. As a result, the minimum load resistance did not exceed the elastic load, even though the reinforcing bars are provided as much as a reinforcing ratio of 0.828%. The value of the P_{min} was found to be approximately 55% of the elastic load. However, the edge distance was not related to the minimum flexural load resistance.

Finally, the ultimate resistance was found to be highly

dependent on the reinforcement ratio, and increased with increasing reinforcement ratio, as depicted in Fig. 9(b). At this stage, only the tensile force of the reinforcement resists the external load, since the crack is almost fully developed. According to the test results, the ultimate resistance increased up to 82% of the elastic load.

3.3 Strain of the titanium bar

Figure 10 shows the strain of the titanium bars. The strain varied linearly until reaching the elastic load, and then the strain started to increase very rapidly until the end of the test. Yielding of the reinforcement occurred in the region (Stage II in Fig. 7) between the peak load and minimum load resistance. Most of the specimens displayed this phenomenon, except for the SP25-90 specimen. However, in some cases, the post-elastic strain could not be monitored due to premature bar fracture. Given that the reinforcement ratio was less than 0.116%, bar fracture occurred immediately after reaching the elastic load.

3.4 Ductility

According to the test results, the titanium bar dramatically contributed to the deformation of the reinforced granite in the case that the reinforcement ratio of 0.148 to 0.524% was provided. The deformation capacity of each specimen can be compared using the ratio of the displacement at yielding to the displacement at failure. This

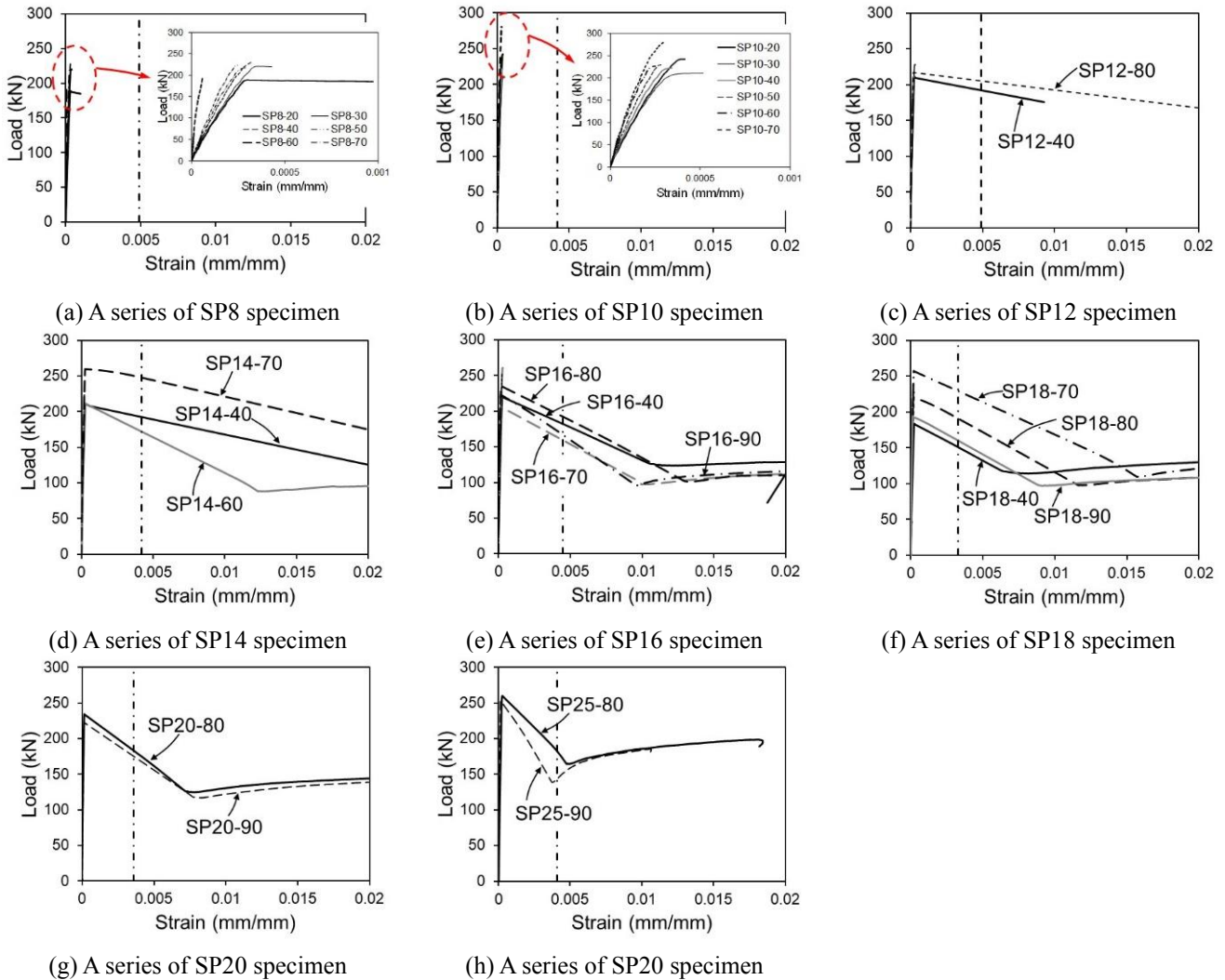


Fig. 10 Strain variation of the titanium bars

study defines the yield displacement as the displacement corresponding to the minimum load resistance since the real yielding point cannot be exactly denoted on the load-displacement curve. Additionally, the displacement at failure is defined as the displacement when the strain of the bar reaches the ultimate strain (ϵ_u). If not, this study uses the displacement at failure as the displacement at the end of the test.

Table 1 summarizes the ductility. The reinforced granite showed good ductility ranging from 1.40 to 10.97 for SP8-40 to SP20-90. The ductility of the reinforced granite increased with increasing reinforcement ratio and edge distance, as can be seen in Fig. 11. For specimens with a reinforcement of 0.148 to 0.524%, the tendency of the increase in ductility is more pronounced. However, the specimens reinforced with the D25 bar showed relatively low ductility, due to the diagonal tension failure (SP25-80), and unexpected failure (SP25-90).

4. Proposed flexural behavior of the reinforced granite

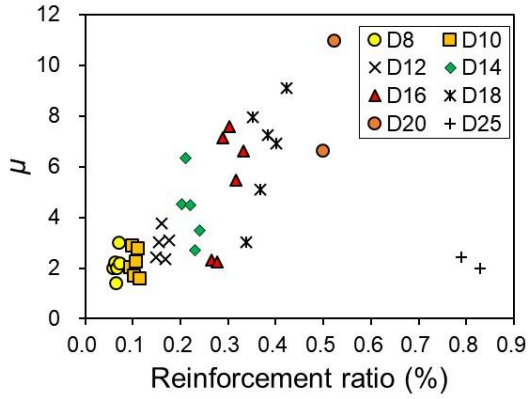
4.1 Basic assumptions for analysis

To propose the flexural behavior of the reinforced granite, several assumptions are needed, as follows: First, reinforced granite subjected to bending moment shows rigid body motion [Fig. 12(a)]. Therefore, ultimate failure occurs due to flexural crack without additional cracks. Second, for granite in compression, linear-elastic stress-strain relationship is assumed, as shown in Fig. 12(b). Additionally, since the compressive strength of the granite is high, the compressive failure of granite does not need to be considered until the end of tests. Third, for titanium bar in tension, a bi-linear stress-strain curve is adopted, as shown in Fig. 12(c). Fourth, a perfect bond is assumed between the surface of the titanium bar, and the epoxy resin in the hole [Fig. 12(d)]. Until ultimate failure, slippage of the reinforcing bar does not occur. Finally, the strain and force distributions at each failure mode are assumed to be as shown in Fig. 13.

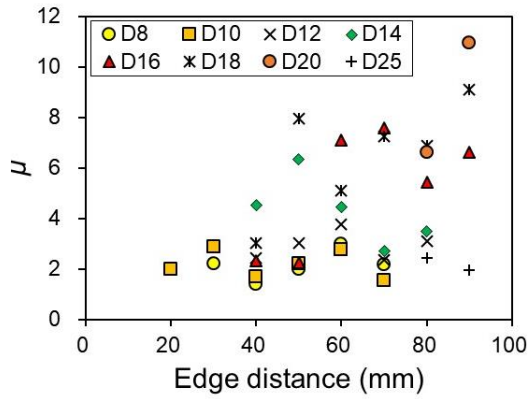
Based on these assumptions, the elastic moment strength, minimum load resistance, and ultimate load resistance are predicted, and the moment-displacement relationship for the design is proposed.

4.2 Predicted moment strength

4.2.1 Predicted elastic moment strength



(a) For reinforcement ratio



(b) For edge distance

Fig. 11 Comparison of ductility

The elastic moment strength determines the suitability of bond performance for adhesives regardless of the reinforcement ratio. This means that the flexural strength at initial cracking, that is, the modulus of rupture (f_{rg}), might be highly related to the elastic moment strength of reinforced granite.

In this study, the modulus of rupture is obtained based on the test results. Using the equation of $f_{rg} = 6M_{el}/bh^2$, the modulus of rupture of epoxy-bonded granite is recommended as the value of 10.08 MPa. Here, M_{el} is the elastic moment strength obtained from the test, while b and h are the width and overall height of the test specimen, respectively. It is noted that the recommended modulus of rupture does not mean that of the plain granite.

Consequently, the predicted elastic moment strength (M_{el_pred}) of the reinforced granite can be obtained as follows:

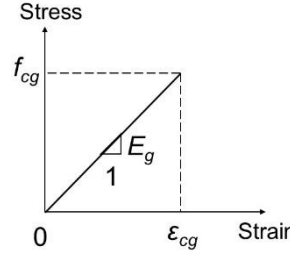
$$M_{el_pred} = f_{rg} Z = 1.68bh^2 \quad (1)$$

where, Z is the section modulus.

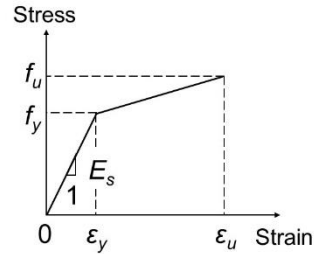
Figure 14(a) shows the ratio of the elastic moment strength obtained from the test to the predicted peak moment strength. As a result, the predicted strength obtained from Eq. (1) shows good agreement with the test results. The average value is 1.0, with a standard deviation of 0.10. Table 4 presents more detailed information about the comparison.



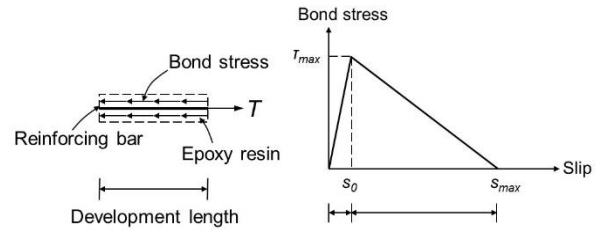
(a) Rigid body motion



(b) Granite in compression



(c) Titanium bar in tension



(d) Bond stress-slip relationship

Fig. 12 Basic assumptions for analysis

4.2.2 Predicted minimum load resistance

The minimum load resistance can be predicted by assuming that the reinforcement has yielded immediately after reaching the elastic moment strength. Therefore, the predicted minimum load resistance (M_{min_pred}) can be considered to be identical to the yield moment strength (M_y) of the reinforced granite, as follows:

$$M_{min_pred} = M_y \quad (2)$$

Hence, the minimum load resistance of the granite reinforced with a single reinforcing bar can be obtained as follows:

$$M_{min_pred} = A_s f_y \left(d - \frac{c_y}{3} \right) \quad (3)$$

where, A_s is the area of the reinforcement, f_y is the yield strength of the titanium bar, d is the effective depth, and c_y is the depth of the neutral axis at yielding.

The depth of the neutral axis can be found as follows:

$$\frac{c_y}{d} = \sqrt{(n\rho)^2 + 2n\rho} - n\rho \quad (4)$$

where, n is the ratio of the modulus elasticity (E_s/E_g) between the reinforcement and granite, ρ is the reinforcement ratio ($= A_s/bd$), and b is the width of the cross section.

Figure 14(b) compares the minimum load resistance between the test results and the predicted values obtained from Eq. (3). The yield strength obtained from the material

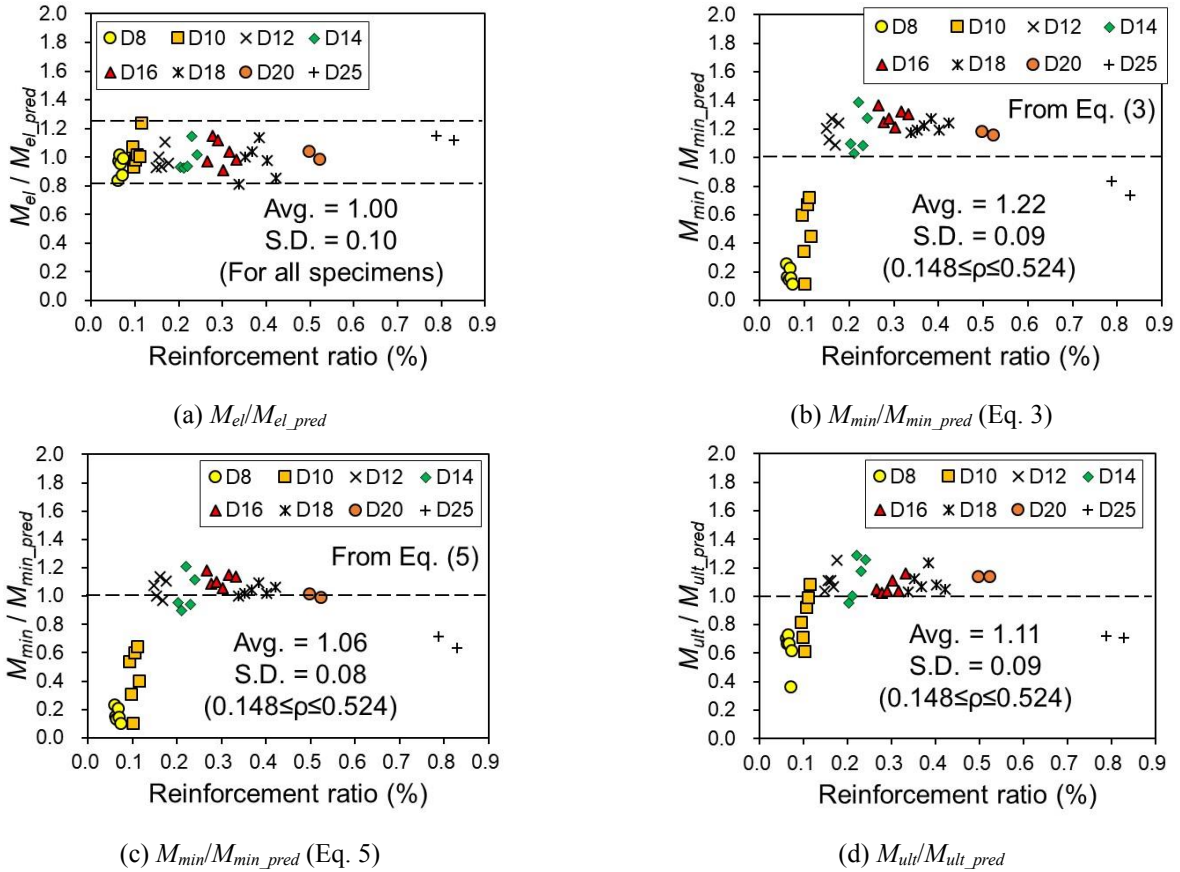


Fig. 14 Comparison of the elastic moment strength between test results and predictions

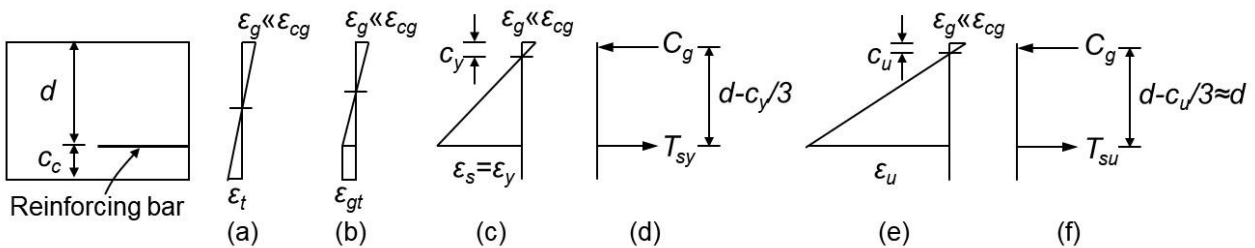


Fig. 13 Strain and force distribution at each failure mode

tests was used in the calculation of the predicted minimum load resistance. In case that the reinforcement ratio ranged from 0.148 to 0.524%, the prediction was less than test results since even though the real yield strengths of each test specimen are measured at the region between the peak load and minimum load resistance (Stage II in Fig. 7). This is because the predicted yield strength was defined as the minimum load resistance (Fig. 7). The average value of the ratio is 1.22, with a standard deviation of 0.09 in this range. On the other hand, the average is 0.91, and the standard deviation is 0.44 for the entire specimens.

Eq. (3) can be simplified as follows:

$$M_{min_pred} = A_s f_y d \tag{5}$$

Figure 14(c) shows the ratio between test results and the predicted obtained from Eq. (5). In the case that the reinforcement ratio is between 0.148 and 0.524%, the

predicted results agree well with the test results. In this range, the ratio of the test result to the predicted is 1.06, with a standard deviation of 0.08.

However, in the low reinforcement ratio ($\rho \leq 0.116\%$), the predictions obtained from Eqs. (3) and (5)

are invalid, due to premature bar fracture. In this case, most of the load resistance vanishes immediately after reaching the elastic load. In addition, when the reinforcement ratio is more than 0.789%, the predictions overestimate the test results. Therefore, the predicted minimum load resistance can be used in the reinforcement ratio ranging from 0.148 to 0.524%.

4.2.3 Predicted ultimate load resistance

According to the test results, the ultimate load resistance is highly related to the tensile strength of the reinforcement. Thus, the predicted ultimate load resistance (M_{ult_pred}) is

Table 4 Comparison of the moment strength between test results and the predicted

Specimens	d_b (mm)	e (mm)	ρ (%)	n (E_s/E_g)	M_{el} / M_{el_pred} (Eq.1)	M_{min} / M_{min_pred} (Eq.3)	M_{min} / M_{min_pred} (Eq.5)	M_{ult} / M_{ult_pred} (Eq.6)	M_{min} / M_{d_el} (Eq.8)
CEP	-	-	-	-	1.18	-	-	-	-
SP8-20	8	20	0.061	1.54	0.83	0.25	0.23	0.70	0.33
SP8-30	8	30	0.063	1.54	0.97	0.16	0.15	0.66	0.20
SP8-40	8	40	0.065	1.54	1.01	0.14	0.13	0.72	0.18
SP8-50	8	50	0.068	1.54	0.96	0.22	0.20	0.67	0.28
SP8-60	8	60	0.071	1.54	0.87	0.16	0.14	0.36	0.20
SP8-70	8	70	0.074	1.54	0.99	0.11	0.10	0.62	0.14
SP10-20	10	20	0.095	1.56	1.07	0.59	0.53	0.82	0.65
SP10-30	10	30	0.099	1.56	0.93	0.34	0.31	0.71	0.37
SP10-40	10	40	0.103	1.56	0.98	0.11	0.10	0.61	0.12
SP10-50	10	50	0.107	1.56	1.01	0.67	0.60	0.92	0.73
SP10-60	10	60	0.111	1.56	1.00	0.72	0.64	0.99	0.78
SP10-70	10	70	0.116	1.56	1.24	0.45	0.40	1.08	0.49
SP12-40	12	40	0.148	1.36	0.93	1.20	1.07	1.04	1.34
SP12-50	12	50	0.155	1.36	1.00	1.13	1.00	1.11	1.25
SP12-60	12	60	0.161	1.36	0.93	1.27	1.14	1.11	1.41
SP12-70	12	70	0.168	1.36	1.11	1.09	0.97	1.07	1.21
SP12-80	12	80	0.176	1.36	0.96	1.24	1.11	1.26	1.38
SP14-40	14	40	0.203	1.65	0.93	1.10	0.96	0.95	1.24
SP14-50	14	50	0.211	1.65	0.93	1.03	0.90	1.00	1.16
SP14-60	14	60	0.220	1.65	0.93	1.39	1.21	1.29	1.57
SP14-70	14	70	0.230	1.65	1.15	1.08	0.94	1.17	1.22
SP14-80	14	80	0.241	1.65	1.02	1.28	1.12	1.26	1.44
SP16-40	16	40	0.266	1.57	0.97	1.36	1.18	1.05	1.56
SP16-50	16	50	0.277	1.57	1.15	1.25	1.09	1.03	1.43
SP16-60	16	60	0.289	1.57	1.12	1.27	1.10	1.04	1.45
SP16-70	16	70	0.302	1.57	0.91	1.21	1.06	1.11	1.39
SP16-80	16	80	0.316	1.57	1.04	1.32	1.15	1.03	1.51
SP16-90	16	90	0.332	1.57	0.98	1.31	1.14	1.16	1.50
SP18-40	18	40	0.338	1.85	0.81	1.17	1.00	1.03	1.14
SP18-50	18	50	0.352	1.85	1.00	1.19	1.02	1.12	1.16
SP18-60	18	60	0.367	1.85	1.04	1.22	1.05	1.07	1.19
SP18-70	18	70	0.384	1.85	1.14	1.28	1.09	1.23	1.24
SP18-80	18	80	0.402	1.85	0.97	1.19	1.02	1.08	1.16
SP18-90	18	90	0.422	1.85	0.86	1.24	1.06	1.05	1.21
SP20-80	20	80	0.499	1.77	1.04	1.18	1.01	1.13	1.21
SP20-90	20	90	0.524	1.77	0.98	1.15	0.99	1.13	1.18
SP25-80	25	80	0.789	1.88	1.15	0.83	0.71	0.72	1.03
SP25-90	25	90	0.828	1.88	1.12	0.74	0.63	0.71	0.91
Avg.					1.00 [†]	0.91 [†] (1.22 [*])	0.80 [†] (1.06 [*])	0.97 [†] (1.11 [*])	1.00 [†] (1.31 [*])
S.D.					0.10 [†]	0.44 [†] (0.09 [*])	0.38 [†] (0.08 [*])	0.22 [†] (0.09 [*])	0.47 [†] (0.14 [*])

Notes: n is calculated using the material properties obtained from the tests. M_{d_el} is the design moment strength obtained using the specified design yield strength of the titanium bar ($f_y = 313.8$ MPa).

[†] For all the test results.

^{*} For the reinforcement ratio ranged from 0.148% (SP12-40) to 0.524% (SP20-90).

proposed as follows:

$$M_{ult_pred} = A_s f_u d \quad (6)$$

Figure 14(d) compares the ultimate load resistance between the test results and the prediction. As a result, the

predicted agreed well with the test data from the reinforcement ratio between 0.148 and 0.524%. In this range, the average value of the ratio is 1.11, with a standard deviation of 0.09. Similarly, when the reinforcement is less than 0.116% or more than 0.789%, the evaluation of the moment strength by Eq. (6) is invalid.

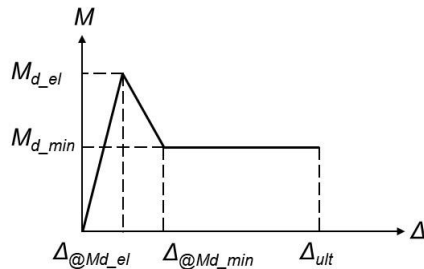


Fig. 15 Load-displacement relationship for the design

4.3 Load-displacement relationship for the design

For the design of reinforced granite with the reinforcement ratio of 0.148 to 0.828%, a tri-linear moment-displacement relationship is proposed based on the basic assumptions assessed in Section 4.1, as can be seen in Fig. 15. The suggested relationship is focused on the elastic moment strength and minimum load resistance. Since the elastic moment strength is related to the bond performance of the adhesive between old and new stones, this value should be considered in the design level, regardless of the reinforcement ratio.

Based on the test results, this study suggests the design elastic moment strength (M_{d_el}) of the reinforced granite as follows:

$$M_{d_el} = f_{rgd}Z \quad (7)$$

where, f_{rgd} is the modulus of rupture of granite bonded with adhesives. Since the special epoxy resin was used as the adhesive in this study, the value of 10.08 MPa is recommended for f_{rgd} . In the case that another adhesive is used in reinforced stone, the value obtained from the tests can be used.

Conversely, the minimum moment capacity of reinforced granite with metal rods should be greater than the minimum load resistance. Thus, the minimum load resistance for the design can be obtained as follows:

$$M_{d_min} = A_s f_{yd} d \quad (8)$$

where, f_{yd} is the specified design yield strength of the reinforcement. Note that the above equation is valid when the reinforcement ratio is greater than approximately 0.15%.

Finally, the ultimate load resistance is assumed to be equal to the minimum load resistance since the load at the ultimate state is found to be higher than the minimum load resistance.

5. Summary and conclusions

This study investigated the flexural behavior of granite reinforced with a threaded titanium bar, depending on the reinforcement ratio and edge distance. The findings obtained from the experimental research are as follows:

- The granite reinforced with a single-titanium bar showed a characteristic flexural behavior as follows: A

crack starts from the contact surface between the epoxy resin and granite, and only a single crack develops until the end of the test. The crack propagates very rapidly, and immediately after reaching the peak load. A sudden drop in load occurs as soon as the load reached the elastic limit. Subsequently, the load starts to increase again due to the strain hardening of the reinforcing bar and reaches the ultimate load. Lastly, a bar fracture occurs at the ultimate limit state.

- According to the test result, when the reinforcement ratio is less than 0.828%, the load capacity of the reinforced granite is governed by the adhesive performance of the epoxy resin. In this range of reinforcement ratio, the peak load is independent of the reinforcement ratio. On the other hand, both the minimum and ultimate load resistance are affected by the reinforcement ratio, which increases as the reinforcement ratio increases.

- The reinforcement affects the deformation capacity of the reinforced granite. The specimens with the reinforcement ratio ranged from 0.148 to 0.524% showed ductile behavior, while brittle failure caused by premature bar fracture occurred at the specimens with a reinforcement ratio of less than 0.116%. These results indicate that the reinforcement ratio of 0.148% needs to be provided to induce ductile behavior.

- The use of ACI 318-14 codes in the determination of the edge distance can be allowed. According to the test results, the bond splitting failure of granite at the edge distance did not occur.

- The predicted elastic moment strength, and minimum and ultimate load resistance were proposed based on the test results and basic assumptions for analysis. As a result, the suggested predictions agreed well with the test data. Finally, the tri-linear moment-displacement relationship for the design of reinforced granite was proposed.

Acknowledgments

The work presented in this paper was sponsored by the National Research Foundation of Korea (NRF) grants (No. 2018R1C1B5045037). The options, findings, and conclusions in this paper are those of the authors and do not necessarily represent those of the sponsors.

References

- National Research Institute of Cultural Heritage (2014), *Conservation Management of Stone Cultural Heritage using Nondestructive Technology*, National Research Institute of Cultural Heritage, Daejeon, Korea.
- Korea Institute of Construction Safety Technology (1998), *Structural Safety Diagnosis for the Stone Pagoda of the Mireuk Temple Site*, Jeonbuk.
- Yang, H.J., Lee, C.H., Choi, S.W. and Lee, M.S. (2006), "Petrological Characteristics and Provenance Presumption for Rock Properties of the Stone Pagoda in Mireuksaji Temple Site, Iksan, Korea", *J. Geological Soc. Korea*, **42**(2), 293-306 (in Korean).
- Kim, S.D., Yi, J.E., Lee, D.S. and Lee, C.H. (2011), "Homogeneity Investigation of Replace Stone for Restoration of the Mireuksaji

- Stone Pagoda in Iksan, Korea”, *J. Conservation Sci.*, **27**(2), 211-222 (in Korean).
- Zambas, C., Ioannidou, M. and Papanicolaou A. (1986), “The use of titanium reinforcement for the restoration of marble architectural members of Acropolis Monuments”, *Proceedings of IIC Congress*, Bologna, 138-141. <https://doi.org/10.1179/sic.1986.31.Supplement-1.138>.
- Zambas, C. (1992), “Structural repairs to the monuments of the Acropolis - The Parthenon”, *Proceedings of the Institution of Civil Engineers*, 166-176. <https://doi.org/10.1680/icien.1992.21497>.
- Kocatürk, T. and Erdoğan, Y.S. (2016), “Earthquake behavior of M1 minaret of historical Sultan Ahmed Mosque (Blue Mosque)”, *Struct. Eng. Mech.*, **59**(3), 539-558. <https://doi.org/10.12989/sem.2016.59.3.539>.
- Demir, A., Nohutcu, H., Ercan, E., Hokelekli, E. and Altintas, G. (2016), “Effect of model calibration on seismic behaviour of a historical mosque”, *Struct. Eng. Mech.*, **60**(5), 749-760. <https://doi.org/10.12989/sem.2016.60.5.749>.
- Nohutcu, H., Hokelekli, E., Ercan, E., Demir A. and Altintas, G. (2017), “Collapse mechanism estimation of a historical slender minaret”, *Struct. Eng. Mech.*, **64**(5), 653-660. <https://doi.org/10.12989/sem.2017.64.5.653>.
- Hamdy, G. A., Kamal, Osama A., El-Hariri, M. O. R. and El-Salakawy, T. S. (2018), “Nonlinear analysis of contemporary and historic masonry vaulted elements externally strengthened by FRP”, *Struct. Eng. Mech.*, **65**(5), 611-619. <https://doi.org/10.12989/sem.2018.65.5.611>
- ACI Committee 318 (2014), *Building Code Requirements for Structural Concrete (ACI 318-14) and Commentary*, American Concrete Institute (ACI), Farmington Hills, MI, USA.
- ASTM C78/C78M-18 (2018), *Standard Test Method for Flexural Strength of Concrete (Using Simple Beam with Third-Point Loading)*, ASTM International, West Conshohocken, PA, USA.
- ASTM C1194-18 (2018), *Standard Test Method for Compressive Strength of Architectural Cast Stone*, ASTM International, West Conshohocken, PA, USA.
- KS F 2519 (2015), *Standard Test Method for Compressive Strength of Nature Building Stone*, Korean Standard Association, Seoul, Korea.
- EN 1992-1-1 (2004), *Eurocode 2: Design of concrete structures - Part 1-1: General Rules and Rules for Buildings*, European Committee for Standardization.
- ASTM E8/E8M-16a (2016), *Standard Test Methods for Tension Testing of Metallic Materials*, ASTM International, West Conshohocken, PA, USA.
- Selwitz, C. (1992), *Epoxy Resins in Stone Conservation*, Research in Conservation 7, Getty Conservation Institute, Marina del Rey, CA, USA.